Multichannel experimental and theoretical approach to the ^{12}C(^{18}O, ^{18}F) ^{12}B single-charge-exchange reaction at 275 MeV. II. Competition between the meson exchange and the sequential transfer in the reaction mechanism

A. Spatafora,[1,*] F. Cappuzzello,[2,1] D. Carbone,[1] M. Cavallaro,[1] G. De Gregorio,[3,4] J. A. Lay,[5] L. Acosta,[6,7] C. Agodi,[1] P. Amador-Valenzuela,[8] J. I. Bellone,[1] G. A. Brischetto,[2,1] D. Calvo,[9] E. R. Chávez Lomelí,[6] I. Ciraldo,[2,1] F. Delaunay,[10] H. Djapo,[11] C. Eke,[12] P. Finocchiaro,[1] S. Firat,[13] M. Fisichella,[14] A. Gargano,[4] A. Hacisalihoglu,[15,16,17] L. La Fauci,[1] H. Lenske,[18] R. Linares,[19] N. Medina,[20] M. Moralles,[20] J. R. B. Oliveira,[21] A. Pakou,[22] L. Pandola,[1] S. S. Perrotta,[23] H. Petrascu,[24] O. Sgouros,[2,1] M. A. G. da Silveira,[25] S. O. Solakci,[13] V. Soukeras,[2,1] G. Souliotis,[26] D. Torresi,[1] S. Tudisco,[1] B. Urazbekov,[27,28] A. Yildirim,[13] and V. A. B. Zagatto[21]
(NUMEN Collaboration)

[1]*Istituto Nazionale di Fisica Nucleare, Laboratori Nazionali del Sud, Catania, Italy*
[2]*Dipartimento di Fisica e Astronomia "Ettore Majorana", Università di Catania, Catania, Italy*
[3]*Dipartimento di Matematica e Fisica, Università della Campania "Luigi Vanvitelli", Caserta, Italy*
[4]*Istituto Nazionale di Fisica Nucleare, Sezione di Napoli, Napoli, Italy*
[5]*Departamento de FAMN, University of Seville, Spain*
[6]*Instituto de Física, Universidad Nacional Autónoma de México, México City, México*
[7]*Instituto de Estructura de la Materia, Consejo Superior de Investigaciones Científicas, 28006 Madrid, Spain*
[8]*Instituto Nacional de Investigaciones Nucleares, Ocoyoacac, México*
[9]*Istituto Nazionale di Fisica Nucleare, Sezione di Torino, Torino, Italy*
[10]*Université de Caen Normandie, ENSICAEN, CNRS/IN2P3, LPC Caen UMR6534, F-14000 Caen, France*
[11]*Ankara University, Institute of Accelerator Technologies, Ankara, Turkey*
[12]*Department of Mathematics and Science Education, Faculty of Education, Akdeniz University, 07058 Antalya, Turkey*
[13]*Department of Physics, Akdeniz University, 07058 Antalya, Turkey*
[14]*Grand Accélérateur National d'Ions Lourds, Boulevard Henri Becquerel, CS 55027, F-14076 Caen, France*
[15]*Institute of Natural Science, Karadeniz Teknik Universitesi, Trabzon, Turkey*
[16]*Department of Physics, Recep Tayyip Erdogan University, Rize, Turkey*
[17]*Turkish Accelerator and Radiation Laboratory, Ankara, Turkey*
[18]*Institut für Theoretische Physik, Justus-Liebig-Universität Giessen, 35392 Gießen, Germany*
[19]*Instituto de Fisica, Universidade Federal Fluminense, Niteroi, Brazil*
[20]*Instituto de Pesquisas Energeticas e Nucleares IPEN/CNEN, São Paulo, Brazil*
[21]*Instituto de Fisica, Universidade de São Paulo, São Paulo, Brazil*
[22]*Department of Physics, University of Ioannina and Hellenic Institute of Nuclear Physics, Ioannina, Greece*
[23]*Lawrence Livermore National Laboratory, Livermore, California 94550, USA*
[24]*Institutul National de Cercetare-Dezvoltare Pentru Fizica si Inginerie Nucleara Horia Hulubei, Bucarest, Romania*
[25]*Centro Universitario FEI, Sao Bernardo do Campo, Brazil*
[26]*Department of Chemistry, University of Athens and Hellenic Institute of Nuclear Physics, Athens, Greece*
[27]*Department of Nuclear Physics and Nanotechnology, L N Gumilyov Eurasian National University, Satpayev Street 2, Astana 010008, Kazakhstan*
[28]*Institute of Nuclear Physics, Laboratory of Low Energy Reactions, Ibragimov Street 1, Almaty 050032, Kazakhstan*

(Received 29 July 2024; revised 10 October 2024; accepted 13 November 2024; published 19 December 2024)

Background: Single-charge-exchange reactions are among the most appropriate nuclear tools to study the response of nuclear systems to isovector interaction. Nowadays, the availability of powerful experimental setups and advanced nuclear models bring the possibility of the complete study of the reaction mechanisms involved in the nuclear reactions, also in the case of heavy projectiles. This new possibility allows one to access valuable information on key nuclear structure aspects, including those embedded in the widely searched neutrinoless double-β decay.

Purpose: We intend to elucidate the main nuclear structure and reaction features involved in the ^{18}O + ^{12}C collision at 275 MeV beam incident energy. In this paper, the main focus is to quantify the competition between the sequential two-step transfer and the direct meson-exchange reaction mechanisms.

*Contact author: alessandro.spatafora@lns.infn.it

Methods: The energy spectra and cross-section angular distributions for the ^{12}C(^{18}O, ^{18}F)^{12}B single-charge-exchange reaction are measured by the MAGNEX magnetic spectrometer in the same experimental setup of the elastic and inelastic scattering and the one-nucleon transfer reaction channels. The cross sections for the sequential two-step transfer and the direct meson-exchange single-charge-exchange reaction mechanisms are evaluated in a single coherent theoretical calculation, using state-of-the-art nuclear structure and reaction theories.

Results: The energy resolution achieved in the study of the ^{12}C(^{18}O, ^{18}F)^{12}B single-charge-exchange reaction allows one to separate the ground-to-ground-state transition and to identify other structures in the measured energy spectra. The coherent sum of the distorted wave Born approximation cross sections of the direct and sequential reaction mechanisms well describes the experimental cross-section angular distributions. The crucial role of the optical model distortion in the scattering of the incoming and outgoing waves was taken into account via the introduction of the coupled-channel local equivalent effective potential.

Conclusions: Advanced nuclear structure and reaction models turned out to be appropriate tools for the detailed analysis of single-charge-exchange reactions originating in heavy-ion collisions. This is of particular relevance in several fields of nuclear physics. Moreover, it is inherent to the challenging project to provide valuable information on neutrinoless double-β decay nuclear matrix elements from single- and double-charge-exchange cross-section measurements.

DOI: 10.1103/PhysRevC.110.064612

I. INTRODUCTION

Over the recent decades, nuclear isovector excitations have been mainly investigated by the $(n, p)/(p, n)$ and the (^{3}He,t)/(d, ^{2}He) single-charge-exchange (SCE) reactions. Considering their selectivity, they have provided key information on nucleon-nucleon isovector interactions [1–6].

Complementary information comes from the use of heavy-ion projectiles in SCE reactions, although their complex many-body nature should be taken into account. The accurate description of the projectile-target potential is needed for both the entrance [initial state interaction (ISI)] and the exit [final state interaction (FSI)] channels. In this case, the quasielastic SCE reactions are localized in the nuclear surfaces of the colliding systems, as a consequence of the strong absorption of the incoming waves in the inner part of heavy nuclei. This is a key aspect of the heavy-ion reaction mechanism since it allows one to transform the full many-body reaction problem into a much simpler one. Indeed, direct reactions as SCE can be treated as small perturbations of the direct elastic scattering, which is typically described by an average local nucleus-nucleus optical potential. For this purpose, modern techniques to build ISI and FSI potentials by double folding integrals of the nucleon-nucleon interaction with the densities of the colliding systems can guarantee a relevant level of accuracy [7–12], provided that the elastic scattering data of the projectile-target system are available at the same incident energy of the SCE reaction cross sections. In a more advanced reaction formalism, the inelastic excitations of the projectile or target can be introduced by solving a system of coupled-channel equations, one for each excitation explicitly considered. The effect of the couplings among different channels can be effectively taken into account via an average local additional complex term to the ISI and FSI, through the introduction of the coupled-channel equivalent potential (CCEP), as suggested in Ref. [13]. The coupling of elastic scattering with inelastic excitations of low-lying collective states of both projectile and target systems has been proven to be important for nucleon transfer reactions, although the effect on SCE has been only partially explored [14].

Accurate knowledge of the ISI and FSI is an indispensable prerequisite for any kind of spectroscopic research on the quantitative level with heavy-ion beams. SCE reactions require, in addition, the careful scrutiny of the reaction mechanism. As discussed in detail, e.g., in [42] and earlier work cited therein, a generic problem of SCE reactions is the competition of collisional nucleon-nucleon (NN) and mean-field-driven sequential proton-neutron transfer processes. Since the two reaction mechanisms populate the same final states, their amplitudes contribute coherently to SCE cross sections. However, as known in principle for a long time, collisional and transfer SCE depend differently on incident energy and on multipolarity and excitation energies of the final states. In particular, the transfer of a proton or neutron from the projectile to the target (stripping process) followed by the transfer to the projectile of a neutron or proton from the target (pick-up process) is a two-step mechanism which populates the same outgoing channel as the direct one-step SCE reaction induced by a two-body isovector nucleon-nucleon interaction. The two-step mechanism is sensitive to the nucleon-nucleus mean field, thus probing, in the first place, single-particle spectroscopy. In contrast, the collisional reaction mechanism relies on isovector NN interaction as mediated by the exchange of the π- and ρ-meson. Since the isovector mesons couple to the nucleons by the same kind of spin-isospin vertices as encountered in weak interactions, the NN mechanism provides the proper operator structures for probing spin-scalar Fermi-type (F) and spin-vector Gamow-Teller-type (GT) nuclear excitations in laboratory experiments under well-defined and reproducible conditions. The properties of NN interactions require one to sum up the NN scattering series to all orders, which is taken care of by using the NN T-matrix rather than elementary Born-type meson-nucleon interactions. In general, the competition of direct one-step and the sequential two-step mechanisms in SCE reactions requires that the reaction amplitudes are summed with their phases, thus generating a specific interference pattern in the differential cross sections. This is a

complication that should be taken into account, especially in heavy-ion-induced SCE reactions, and possibly minimized by an appropriate choice of the experimental conditions. From the theory point of view, this issue has been extensively debated in the past [15–22], with major advances achieved thanks to the development of microscopic approaches for the data interpretation.

To our knowledge, the only reported case where a fully consistent calculation includes one- and two-step routes is found in Ref. [19], in which second-order distorted-wave Born approximation (DWBA) theory and suitable shell-model wave functions, used to provide all the necessary nuclear structure inputs, were adopted to analyze the ^{12}C(^{12}C, ^{12}N)^{12}B SCE reaction. As a general finding, the two-step mechanisms tend to be small at incident energies far above the Coulomb barrier, although the transition from one-step to two-step dynamics as a function of the incident energy is very dependent on the specific SCE reaction as well as on the particular states that are considered. This has been reported in (^{12}C, ^{12}B), (^{12}C, ^{12}N), (^{13}C, ^{13}N) [23,24], and (^{7}Li, ^{7}Be) reactions [21,25], and explored at different energies from 5 to 70 A MeV and on different targets [26–31].

An interesting aspect of heavy-ion-induced SCE reactions is that a significant amount of linear momentum is transferred to the final asymptotic state, even at forward angles. This feature is considered a drawback of heavy-ion-induced SCE reactions, when the typical focus is to characterize the $L = 0$ modes, namely, the GT one. However, this property is interesting to probe the nuclear response to the higher multipoles of the isospin (F-like) and spin-isospin (GT-like) operators, since neither β-decay nor light-ion-induced SCE reactions effectively access such high multipolarities. Nowadays, much interest is given to this aspect of nuclear response for its implications in neutrinoless double-β ($0\nu\beta\beta$) decay matrix elements [32,33], where high-order multipoles are considered to contribute the most [34]. Thus, the exploration of heavy-ion-induced SCE reactions has recently regained interest, with the consequent need to develop suitable experimental techniques and advanced theoretical analysis [35,36] for a detailed description of the data. A recent review on the field is found in Ref. [35].

Among the heavy-ion-induced SCE reactions, a promising one is the (^{18}O, ^{18}F). The ^{18}F ($Z = 9$, $N = 9$) nucleus is the intermediate system between the mirror ^{18}O ($Z = 8$, $N = 10$) and ^{18}Ne ($Z = 10$, $N = 8$) nuclei. In terms of spin-isospin symmetry, the ^{18}O $J^\pi = 0^+$ ground state ($T = 1$; $T_z = 1$), the $J^\pi = 0^+$ ^{18}Ne ground state ($T = 1$; $T_z = -1$), and the $J^\pi = 0^+$ excited state of ^{18}F ($T = 1$; $T_z = 0$) at 1.042 MeV are isobaric analog states (IASs) of the $T = 1$ isospin-triplet $S = 0$ spin-singlet state, while the $J^\pi = 1^+$ ground state of ^{18}F ($T = 0$; $T_z = 0$) is the $T = 0$ isospin-singlet $S = 1$ spin-triplet state. The strong shell closure of the ($Z = 8$, $N = 8$) ^{16}O doubly magic nucleus emphasizes the role of the two-valence nucleons in the determination of such a symmetric scheme. Thus, one can expect that the symmetry of the nuclear interaction between free pairs of nucleons is directly reflected in the spin-isospin multiplets of ^{18}O, ^{18}F, and ^{18}Ne. Hints of this dynamics come from the super-allowed β-decay Gamow-Teller transitions from the $J^\pi = 1^+$ ground state of ^{18}F to the ^{18}O ground state ($\log ft = 3.570$), and from the $J^\pi = 0^+$ ground state of ^{18}Ne to the ^{18}F ground state ($\log ft = 3.091$) [37]. Experimentally, one can access the pure spin-isospin $\sigma\tau^-$ (GT-like) response of the target nucleus by selecting the (^{18}O, ^{18}F$_{\text{g.s.}}$) transition in the energy spectra. Here, τ^- indicates the isospin lowering operator. Similarly, the pure isospin τ^- (F-like) response is selected by gating on the (^{18}O, ^{18}F$^*_{1.042\text{MeV}}$) transition in the spectra. Such interesting properties were recognized long ago in the first attempts to explore the ^{28}Si(^{18}O, ^{18}F)^{28}Al reaction at the Saclay [38] and the HHIRF Oak Ridge [39] facilities and the ^{36}S(^{18}O, ^{18}F)^{36}P reaction at the ANU Canberra [40] laboratory. The selectivity of the reaction and the competition between one- and two-step reaction mechanisms were discussed in such articles. However, due to the limitations in the computing power and theoretical approaches adopted for the data analyses, large scaling factors were necessary to reproduce the magnitude of the measured cross sections, thus preventing the reaching of firm conclusions. In addition, the typically high level density in SCE reaction data, which often does not allow one to isolate transitions to individual states of the residual nucleus, has, for a long time, hindered the actual use of the (^{18}O, ^{18}F) as a spectroscopic tool for nuclear structure studies.

Recently, a renewed interest for (^{18}O, ^{18}F) SCE reaction is growing by the systematic use of the ^{18}O beam for the NUMEN project [41,42]. The main goal is the study of the (^{18}O, ^{18}Ne) double-charge-exchange (DCE) reactions for their link with $0\nu\beta\beta$ decay [41,43]. Nonetheless, the multichannel approach proposed in order to extract constrained nuclear structure information requires that all the direct quasielastic reactions stemming from the collision of the ^{18}O beam with the target are consistently studied. In particular, the (^{18}O, ^{18}F) should be described with an unprecedented level of accuracy. In fact, both the one- and two-step reaction mechanisms feeding the (^{18}O, ^{18}F) provide important information about the meson exchange and the mean-field dynamics, respectively, which are then used for the analysis of the (^{18}O, ^{18}Ne) reaction data. New studies on the (^{18}O, ^{18}F) have been performed in recent years in Refs. [14,44]. In particular, the ^{40}Ca(^{18}O, ^{18}F)^{40}K reaction at 270 MeV beam incident energy is analyzed in terms of the one-step contribution to the cross section in Ref. [14] using nuclear structure inputs, namely, transition densities, from quasiparticle random phase approximation (QRPA). The same reaction is investigated in Ref. [44] within a pure two-step approach, adopting spectroscopic amplitudes (SAs) from a large-scale shell model. Although the conclusions of the two complementary studies fairly match each other, it is uncomfortable that the nuclear structure inputs come from different sources and that the two reaction mechanisms are studied in separate calculations, thus ignoring their interference.

For the sake of investigating the (^{18}O, ^{18}F) reaction dynamics, keeping the uncertainties from the nuclear structure model as small as possible, we decided to explore the ^{12}C(^{18}O, ^{18}F)^{12}B reaction at 275 MeV. Indeed, the ^{12}C $\rightarrow$ ^{12}B SCE transitions have been investigated through several probes [18–21] and the nuclear shell model provides quite accurate results for such nuclei. The reliability of the nuclear

structure inputs allows us to do a more refined job with the reaction model, where one- and two-step mechanisms are consistently calculated and their reaction amplitudes, including the phases, are coherently summed in the cross-section determination. In addition, the role of couplings in the ISI is estimated in average in a complete SCE analysis by the CCEP approach.

Here we report about the main achievements of this study. In particular, we analyze recent differential cross-section data from the NUMEN project [41] within the aforementioned multichannel approach [43]. It should be mentioned that the elastic and inelastic scattering, the neutron stripping and the proton pick-up reactions analyses were published in Ref. [45], which we refer to for details of the experimental setup and theoretical analysis, which, in the spirit of the multichannel methodology, are largely in common with this article.

The article is organized as follows: The experiment and the measured energy spectra are presented in Sec. II, the theoretical framework is described in detail in Sec. III, and the comparison of the calculated and measured cross sections is discussed in Sec. IV, followed, in Sec. V, by the conclusions.

II. EXPERIMENTAL SETUP AND RESULTS

The experiment was performed at the Istituto Nazionale di Fisica Nucleare, Laboratori Nazionali del Sud (INFN-LNS) in Catania, using the ^{18}O ion beam accelerated by the K800 Superconducting Cyclotron at 275 MeV (15.3 AMeV) bombarding energy and the MAGNEX large acceptance magnetic spectrometer [46]. The magnetic fields of the MAGNEX dipole and quadrupole magnets were set in order to transport the $^{18}F^{9+}$ ions, corresponding to the ejectiles of the SCE reaction channel, in the domain of momenta covered by the MAGNEX focal plane detector (FPD) [47]. The two self-supporting ^{12}C targets used during the measurements (60 $\pm$3 μg/cm^2 and 200 $\pm$10 μg/cm^2 thick) were located at the object point of the magnetic spectrometer whose optical axis was oriented, compared to the beam direction, at $\theta_{opt} = 7.5°$, 8°, and 13.5°. The details of the experimental setup and data reduction have been previously described in Ref. [45]. It is worth emphasizing that all the reaction channels therein presented were measured in the same experimental conditions and that the evaluation of the absolute cross sections was conducted adopting the multichannel approach that allows one to minimize the sources of systematic uncertainty.

The excitation energy E_x was calculated as the difference $Q_0 - Q$, where Q_0 is the ground-to-ground-state Q value, and Q is the Q value obtained by the missing mass technique based on relativistic kinematic transformations. The E_x spectrum for the ^{12}C(^{18}O, ^{18}F) ^{12}B charge-exchange reaction at 275 MeV beam incident energy in the angular region $8° < \theta_{lab} < 10°$ is shown in Fig. 1. Heavy-ion charge-exchange reactions populating odd-odd systems both in the ejectile and residual nuclei typically produce energy spectra characterized by high level density. This is the case of the ^{40}Ca(^{18}O, ^{18}F) ^{40}K [14] and the ^{116}Cd(^{20}Ne, ^{20}F) ^{116}In [48] reactions, recently studied in similar experimental conditions. In these cases, it was not possible to identify transitions towards isolated states in the

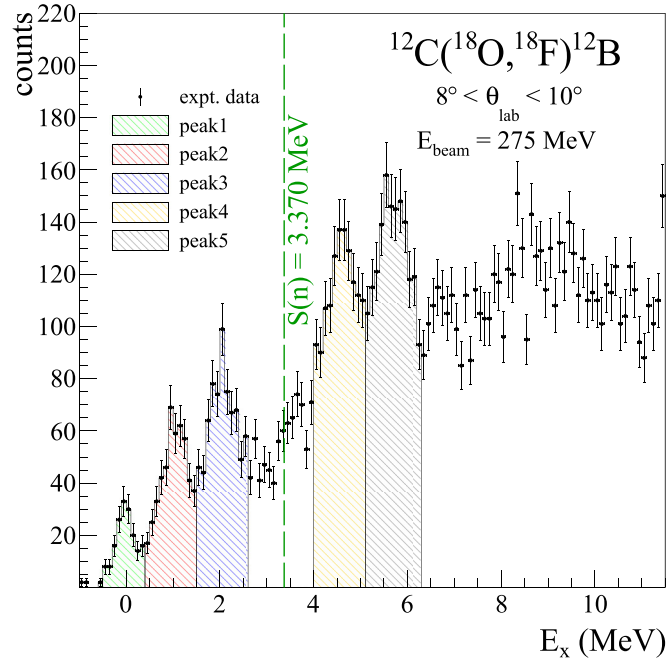

FIG. 1. ^{12}C(^{18}O, ^{18}F) ^{12}Be single-charge-exchange energy spectrum at 275 MeV beam incident energy and $8° < \theta_{lab} < 10°$. Hatched areas indicate the regions of interest for the study of the cross-section angular distributions as labeled in the legend. Dashed green line indicates the S_n one-neutron emission threshold.

spectra, often appearing as poorly structured and mainly dominated by the rapid growth in the final nuclei level density. In the present case, in which the lighter ^{12}B residual nucleus is under study, the level density of nuclei at the exit channel is still manageable, allowing one to identify several structures in the spectra. Despite the fact that the combination of the states for the ejectile and residual nuclei generates hundreds of transitions in the first MeVs of the spectrum, five peaks are clearly visible and three of them are below the ^{12}B one-neutron emission threshold S_n at 3.370 MeV.

The first peak in Fig. 1 corresponds to the $0^+ \rightarrow 1^+$ ground-to-ground-state transition undertaken in both the targetlike and projectilelike nuclei. The energy resolution $\delta E_x \approx$ 0.6 MeV was enough to separate this transition from the ones populating the first excited states, expected to be at about 1 MeV, where a second peak appears in the spectrum. In this second peak, contributions to the overall yield are expected to come from the transitions to the 3^+0.937, 0^+1.042, 0^-1.080, and 5^+1.121 MeV states of the ^{18}F ejectile, and the 2^+0.953 MeV state of the ^{12}B residual nucleus. In the region of the third peak, at about 2 MeV, contributions could come from the simultaneous excitation of the ^{12}B 2^+ state at 0.953 MeV and the 3^+, 0^+, 0^-, and 5^+ ^{18}F states at 0.937, 1.042, 1.080, and 1.121 MeV, respectively. Other contributions could also come from the population of the ^{12}B 2^- state at 1.674 MeV, although the centroid of this structure suggests a minor role for this last transition. The two most prominent peaks are located above S_n overlying the continuous spectrum in the ^{12}B unbound states region. The fourth peak located at $E_x \approx$

4.5 MeV was already observed in other charge-exchange experiments on the ^{12}C target [20,49] and it was interpreted as the excitation of the 2^- and 4^- unnatural parity states of ^{12}B at 4.460 and 4.524 MeV, respectively. The distance of about 1 MeV among peaks 4 and 5 suggests that the latter is a satellite of the former, simultaneously populating the ^{18}F states at ≈1 MeV.

The absolute cross-section angular distributions are shown in Fig. 2. These were extracted for the transitions to the five peaks without any renormalization factor applied to the data [45]. The yield was integrated in the hatched regions highlighted in Fig. 1 in angular slices from 0.3° to 1.2°, moving from forward to backward angles in the $3.5^\circ < \theta_{\rm lab} < 14.3^\circ$ angular range. In SCE, it would have been interesting to measure the experimental cross sections at very small angles, where most of the reaction strength is concentrated. However, from the experimental side, this task is quite demanding in (^{18}O, ^{18}F) SCE due to the hydrogen contamination commonly present in the targets. In fact, the large cross section of the $p(^{18}\mathrm{O}, ^{18}\mathrm{F})n$ nuclear reaction is an unavoidable background source and makes it prohibitive to extract reliable energy spectra for the $^{12}\mathrm{C}(^{18}\mathrm{O}, ^{18}\mathrm{F})^{12}\mathrm{B}$ reaction at angles smaller than the $\theta_{\rm lab} = 3.13^\circ$ that is the maximum angle in the $p(^{18}\mathrm{O}, ^{18}\mathrm{F})n$ inverse kinematics. Experimental points in the angular regions in overlap between different setups were estimated by the weighted average of the different measured values. The error bars in Fig. 2 include uncertainties coming from the statistical contribution and solid angle estimation. An overall systematic uncertainty of about 10%, due to the determination of charge collection and target thickness, is common to all data points in the angular distributions and is not included in the error bars. The angular resolution is $\delta\theta_{\rm c.m.} \approx 0.8^\circ$, allowing one to bring to light the eventual diffracting oscillation pattern in the angular distributions [45].

III. THEORETICAL ANALYSIS

The SCE nuclear reaction considered in this work can be described according to the scheme

$$ {}^{a}_{z}\mathrm{a} + {}^{A}_{Z}\mathrm{A} \rightarrow {}^{a}_{z+1}\mathrm{b} + {}^{A}_{Z-1}\mathrm{B}, \tag{1}$$

which maintains the distribution of masses, but changes the charge partition by a balanced redistribution of protons and neutrons. For such a process, the cross section is defined as

$$ d\sigma_{\alpha\beta} = \frac{m_\alpha m_\beta}{(2\pi\hbar^2)^2}\frac{k_\beta}{k_\alpha}\frac{1}{(2J_a+1)(2J_A+1)} \times \sum_{M_a,M_A\in\alpha;M_b,M_B\in\beta} |\mathcal{M}_{\alpha\beta}(\mathbf{k}_\alpha,\mathbf{k}_\beta)|^2 d\Omega, \tag{2}$$

where $\mathbf{k}_\alpha$ ($\mathbf{k}_\beta$) and m_α (m_β) denote the relative 3-momentum and reduced mass in the entrance (exit) $\alpha = a, A$ ($\beta = b, B$) channel, respectively.

As discussed, SCE reactions can proceed through two different paths consisting in the sequential two-step transfer of nucleons and in a direct meson-exchange process, mediated by the isovector parts of the nucleon-nucleon interaction.

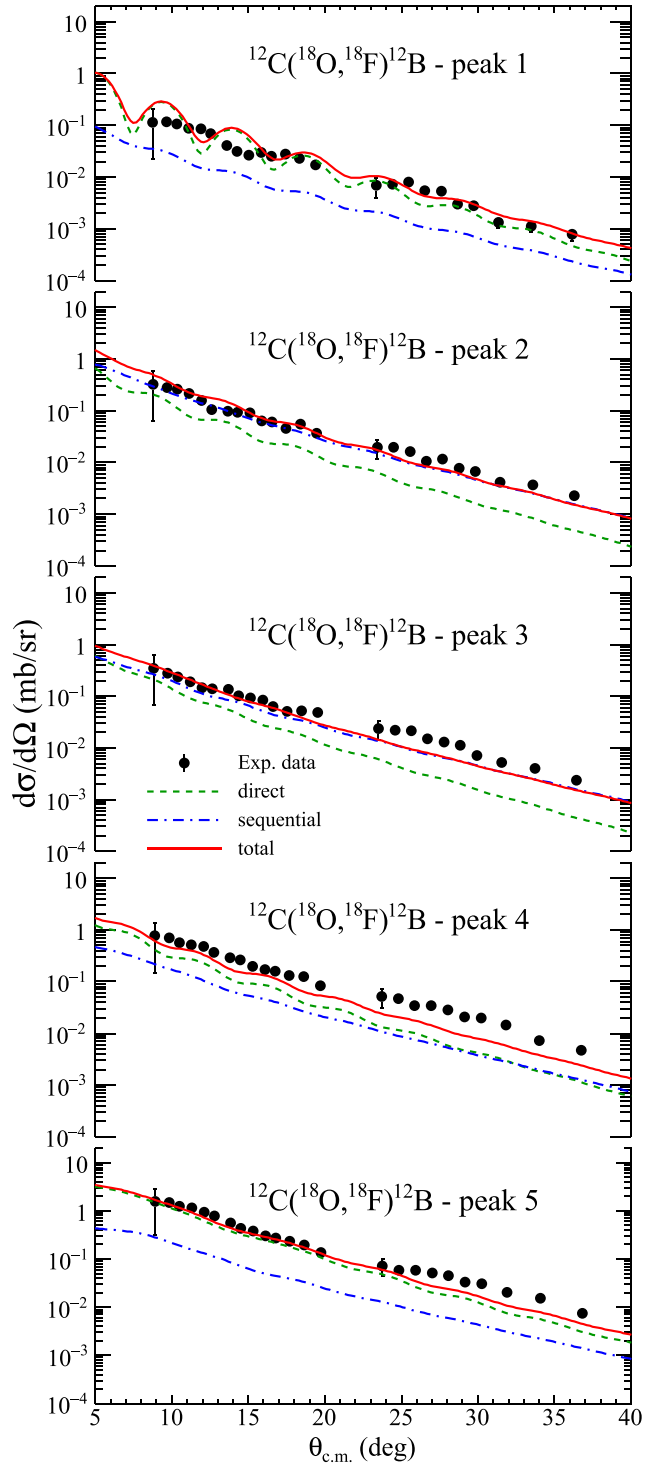

FIG. 2. Experimental cross-section angular distribution of the $^{12}\mathrm{C}(^{18}\mathrm{O}, ^{18}\mathrm{F})^{12}\mathrm{B}$ single-charge exchange at 275 MeV beam incident energy associated with the five peaks indicated in the spectrum of Fig. 1. DWBA theoretical calculations obtained adopting the CCEP are shown for the direct meson exchange (green dashed line), the two-step sequential nucleon transfer (blue dot-dashed line), and the coherent sum of both kinds of reaction amplitudes (red continuous line). All the theoretical curves are folded with the experimental angular resolution.

The full SCE is expressed by the sum of the two reaction amplitudes,

$$\mathcal{M}_{\alpha\beta}(\mathbf{k}_\alpha, \mathbf{k}_\beta) = \mathcal{M}^D_{\alpha\beta}(\mathbf{k}_\alpha, \mathbf{k}_\beta) + \mathcal{M}^S_{\alpha\beta}(\mathbf{k}_\alpha, \mathbf{k}_\beta), \quad (3)$$

where both $\mathcal{M}^D_{\alpha\beta}(\mathbf{k}_\alpha, \mathbf{k}_\beta)$ and $\mathcal{M}^S_{\alpha\beta}(\mathbf{k}_\alpha, \mathbf{k}_\beta)$, i.e., the direct and sequential reaction amplitudes, have both real and imaginary components. In this framework, the proper treatment of the interference between the two reaction mechanisms requires accurate tests of its consistency [36,43].

Furthermore, the study of the complete reaction mechanism also implies a data analysis in a consistent nuclear structure framework. In the present work, the nuclear structure information for the projectilelike and targetlike nuclei are treated in the large-scale shell-model framework, used to provide the required SAs and one-body transition densities (OBTDs).

The calculations were performed making use of the FRESCO code [50]. Both contributions to the process under study were computed, as is customary, through partial wave decomposition of the reaction amplitudes and multipole expansion of the relevant form factors [51]. The meson-exchange and sequential transfer calculations were performed for a large number of transitions, to analyze the cross-section angular distributions shown in Fig. 2. In order to consistently treat the interference between the two reaction mechanisms in the framework of a full comprehensive calculation, the two calculations were performed simultaneously.

A. Two-step transfer reaction mechanism

The two-step SCE reaction mechanism is a two-nucleon sequential transfer process populating the SCE final partition. Two different sequences of neutron and proton transfer compete to populate the same SCE partition and, in the case of our ^{12}C(^{18}O, ^{18}F)^{12}B reaction, the τ^+ direction in the target selects the neutron stripping and the proton pick-up as intermediate steps for the two possible reaction patterns. We will refer to them using the *np*-sce and the *pn*-sce acronyms. This scenario is described by the following expressions:

$$\begin{aligned} pn-sce \quad & {}^{a}_{z}\mathrm{a} + {}^{A}_{Z}\mathrm{A} \rightarrow {}^{a+1}_{z+1}\mathrm{c} + {}^{A-1}_{Z-1}\mathrm{C} \rightarrow {}^{a}_{z+1}\mathrm{b} + {}^{A}_{Z-1}\mathrm{B}, \\ np-sce \quad & {}^{a}_{z}\mathrm{a} + {}^{A}_{Z}\mathrm{A} \rightarrow {}^{a-1}_{z}\mathrm{d} + {}^{A+1}_{Z}\mathrm{D} \rightarrow {}^{a}_{z+1}\mathrm{b} + {}^{A}_{Z-1}\mathrm{B}, \end{aligned} \quad (4)$$

where partitions $\alpha = \{a, A\}$, $\beta = \{b, B\}$, $\gamma = \{c, C\}$, and $\delta = \{d, D\}$ are involved. In the reaction under study, the ^{17}O + ^{13}C and the ^{19}F + ^{11}B systems are involved as intermediate partitions. For such systems, a finite model space has been defined according to the analysis described in Ref. [45].

The *p-sd-mod* interaction [53] is adopted for the shell-model calculations for both projectile and target nuclei. It assumes ^{4}He as the inert core with the valence protons and neutrons in the $1p2s1d$ orbits, where 1 refers to the lowest possible principal or radial quantum number. The comparison between theoretical and experimental excitation energies of the low-lying states for the ^{18}F and ^{12}B nuclei is shown in Table I of Ref. [52], while the same comparison for the other nuclei involved in the complete network of nuclear reactions is included in Table VII of Ref. [45]. The SAs for the first step of the one-nucleon transfer calculations are those listed in Tables VIII– XI of Ref. [45]. The SAs related to the $\langle ^{17}\mathrm{O}|^{18}\mathrm{F}\rangle$ and $\langle ^{13}\mathrm{C}|^{12}\mathrm{B}\rangle$ overlaps involved in the second step of the *np*-sce nuclear reaction are listed in Tables II and III in Ref. [52], respectively, while those related to the $\langle ^{19}\mathrm{F}|^{18}\mathrm{F}\rangle$ and $\langle ^{11}\mathrm{B}|^{12}\mathrm{B}\rangle$ overlaps, involved in the *pn*-sce path, are listed in Tables IV and V of Ref. [52], respectively. As a compromise between the computation time and reliability of the calculations, not all of the listed SAs have been included in the reaction calculations. The selection of the included states has been done considering the dominant transitions in the first step, according to the measured cross sections, as shown in Fig. 3. For the second step, only the couplings with SAs larger than 0.1 were taken into account. The coupling schemes for the *pn*-sce and *np*-sce paths are shown in Fig. 3, where the couplings in the first and second steps are indicated and are assumed to be one-way only.

Single-particle wave functions were calculated considering the transferred particle bound to the core by means of a Woods-Saxon potential. The depth of the potential was adjusted to reproduce the separation energy of the transferred particle, whereas the radius and the diffuseness were set to typical values [54], recently adopted in other ^{18}O-induced transfer reactions [55–59]. The assumptions for the the first step of the sequential transfers were presented in Ref. [45] and they remained unchanged in this case. For the second step, the reduced radii and diffuseness of 1.26 and 0.7 fm, respectively, were assumed both for the projectilelike ^{17}O + p, and ^{18}F + n systems. In the case of the targetlike ^{12}B + p and ^{11}B + n systems, the 1.25 and 0.65 fm values were adopted for the radii and diffuseness parameters, respectively.

All of the mentioned ingredients were introduced in a single full complex remnant calculation including, in addition to the SCE reaction channel, the elastic and inelastic scattering within the initial partition, and the one-neutron and one-proton transfer within the intermediate ones. The prior-post representation, where the second-order DWBA nonorthogonality term is exactly zero [60], was adopted for the sequential transfer calculations.

Examples of the *pn* and *np* sequential transfer SCE calculations, obtained within the second-order DWBA approach described here, are shown together with their coherent sum in Fig. 4. The states shown therein are those having the largest cross section from the sequential transfer reaction mechanism and are related to the ^{12}C(^{18}O, ^{18}F$_{0.937}(3^+)$)^{12}B$_{\mathrm{g.s.}}(1^+)$ and the ^{12}C(^{18}O, ^{18}F$_{0.937}(3^+)$)^{12}B$_{0.953}(2^+)$ transitions. The two states, as described in Sec. IV, contribute the most in the yield of peak 2 and peak 3 of the spectrum.

B. One-step meson-exchange reaction mechanism

The collisional NN mechanism is described sufficiently well as a one-step process by DWBA theory. The finite-range character of meson-exchange interactions is taken into account. An antisymmetrized NN T-matrix is used, as discussed in Ref. [61]. Knock-on exchange processes are treated as usual by local pseudopotentials. In Refs. [36,61], the theoretical formalism was presented and extensively discussed. For the

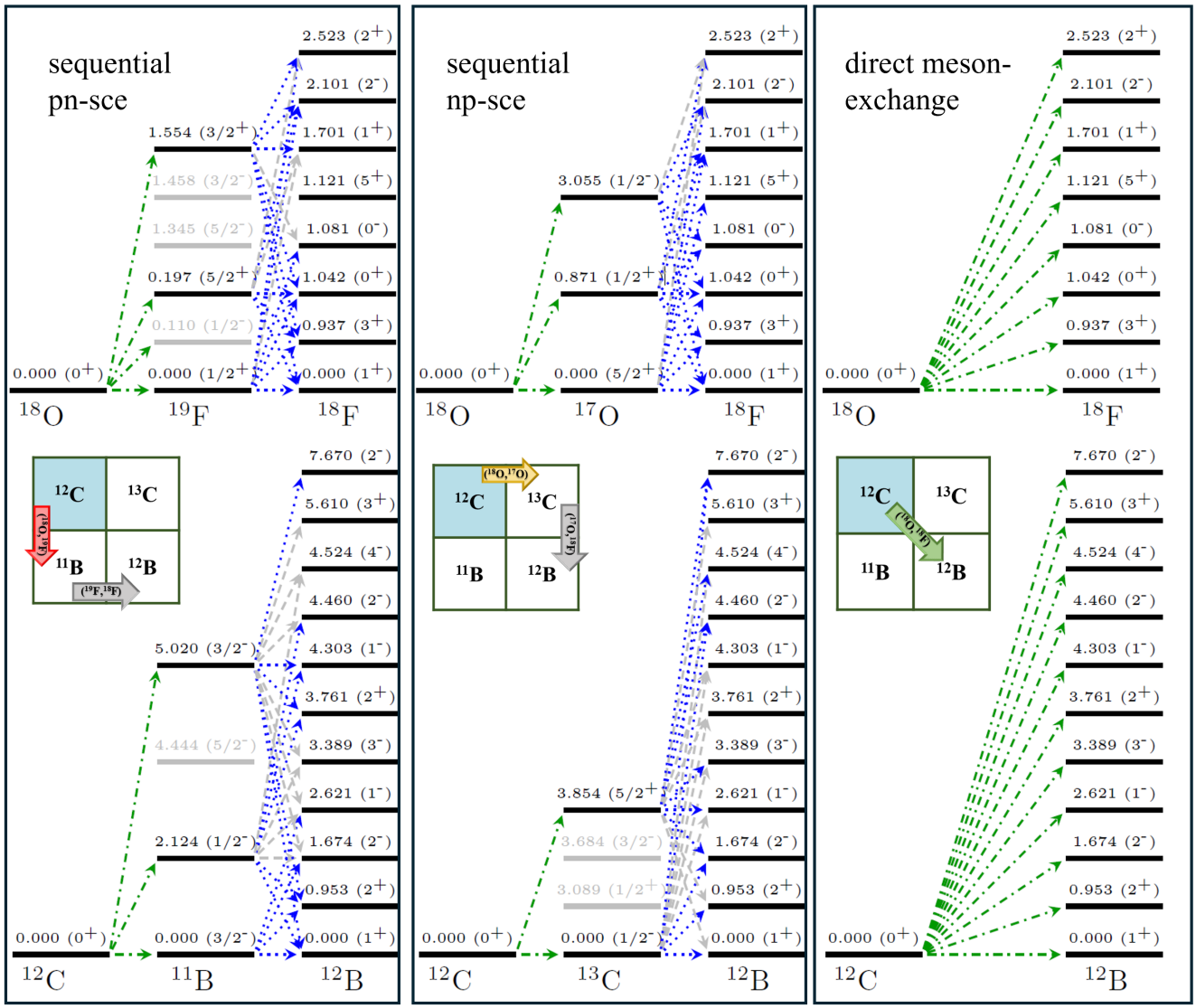

FIG. 3. Coupling scheme adopted for the *pn*, *np* sequential transfer and meson-exchange paths in the ^{12}C(^{18}O, ^{18}F) ^{12}B SCE reaction calculation for the projectilelike and targetlike nuclei. Couplings considered in the first and second steps of the DWBA calculations are indicated by the dash-dotted green and dotted blue arrows, respectively. Gray arrows, connecting the intermediate to the final partitions, correspond to transitions with SAs smaller than 0.1 (see tables in Ref. [52]) and were neglected in the present calculations. Excitation energies in MeV and J$^{\pi}$ of each of the involved states are indicated.

sake of completeness, in the following section, the relevant formulas are collected and summarized.

In SCE, it is useful to express the nuclear scattering amplitude for the direct meson exchange $\mathcal{M}^{D}_{\alpha\beta}$ in the momentum space, to separate for the projectile and target coordinates,

$$\begin{aligned}\mathcal{M}^{D}_{\alpha\beta}(\mathbf{k}_\alpha,\mathbf{k}_\beta) = &\sum_{J_1M_1,J_2M_2,LM}(J_aM_aJ_bM_b|J_1M_1)\\ &\times(J_AM_AJ_BM_B|J_2M_2)(J_1M_1J_2M_2|LM)\\ &\times\int d^3p N_{\alpha,\beta}(\mathbf{k}_\alpha,\mathbf{k}_\beta,\mathbf{p})i^L\\ &\times Y_{LM}(\hat{\mathbf{p}})M^{(J_aJ_A,J_bJ_B)}_{LJ_1J2}(p^2),\end{aligned}\tag{5}$$

where

$$\begin{aligned}M^{(J_aJ_A,J_bJ_B)}_{LJ_1J2}(p^2) = \sum_{ST}\delta_{T1}\big[&V^{(C)}_{ST}(p^2)F^{J_1J_2}_{LS}(p^2)\\ &+\delta_{S1}V^{(Tn)}_{T}(p^2)H^{J_1J_2}_{L1}(p^2)\big]\end{aligned}\tag{6}$$

and $N_{\alpha,\beta}(\mathbf{k}_\alpha,\mathbf{k}_\beta,\mathbf{p})$ is the distortion factor, i.e., the Fourier transform of the distorted waves product in the initial and final partitions, accounting for the reaction dynamics of the process. The $M^{(J_aJ_A,J_bJ_B)}_{LJ_1J2}(p^2)$ reduced matrix element includes both the central (C) and the tensor (Tn) components of the nucleon-nucleon interaction, the latter being relevant only in the case of spin-flip ($S=1$) transitions. The $F^{J_1J_2}_{LS}(p^2)$ and $H^{J_1J_2}_{L1}(p^2)$ are the reduced multipole form factors defined by

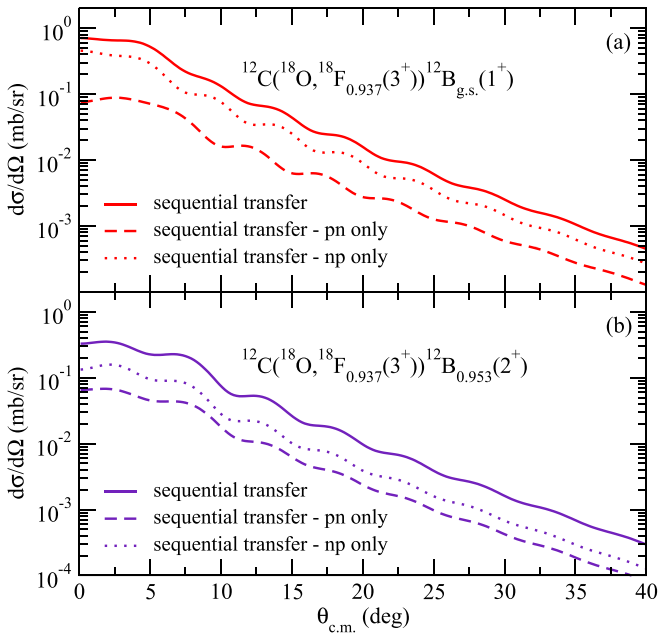

FIG. 4. Theoretical angular distributions of differential cross sections for the (a) ^{12}C(^{18}O, ^{18}F$_{0.937}(3^+)$) ^{12}B$_{g.s.}(1^+)$ and (b) ^{12}C(^{18}O, ^{18}F$_{0.937}(3^+)$) ^{12}B$_{0.953}(2^+)$ SCE reactions at 275 MeV beam incident energy. The curves are evaluated within the two-step DWBA calculations of the sequential transfer SCE reaction mechanism adopting the CCEP. The *pn* (dashed lines) and *np* (dotted lines) paths and their coherent sum (continuous line) are shown separately for each transition.

the expressions

$$F_{LS}^{J_1J_2}(p^2) = \sum_{L_1L_2} A_{LS}(L_1L_2, J_1J_2) f_{L_1SJ_1}^{(ab)}(p^2) f_{L_2SJ_2}^{(AB)}(p^2), \quad (7)$$

$$H_{L1}^{J_1J_2}(p^2) = \sum_{L_1L_2L'} B_{LL'}(L_1L_2, J_1J_2) f_{L_1 1J_1}^{(ab)}(p^2) f_{L_2 1J_2}^{(AB)}(p^2). \quad (8)$$

The total angular momentum transfer in the projectile (target) system is given by J_1 (J_2), defining the set of multiple components contributing to the reaction in which the initial $J_{a,A}$ and final $J_{b,B}$ states are involved. These multipoles carry the substructures given by the coupling of the orbital L_1 (L_2) and spin S_1 (S_2) angular momentum in the projectile (target). The $f_{L_1SJ_1}^{(ab)}(p^2)$ and $f_{L_2SJ_2}^{(AB)}(p^2)$ are the Fourier-Bessel transform of the radial transition densities $\rho_{L_1SJ_1}^{(ab)}(r)$ and $\rho_{L_2SJ_2}^{(AB)}(r)$ for the projectile and target, respectively.

The evaluation of transition densities requires the knowledge of the structure of the initial and final nuclear states, establishing the connection to nuclear structure theory, and for this reason they are the elements of central importance for the spectroscopy of the charge-exchange process. In the present work, transition densities have been calculated using the formalism adopted in Refs. [18,19,62], in which the radial transition densities were expanded in terms of the OBTDs. In the case of the projectile,

$$\rho_{L_1SJ_1}^{(ab)}(r) = \sum_{\xi_i\xi_k} C_{L_1SJ_1}^{j_il_ij_kl_k}(ab) \varphi_{\xi_i}^b(r_1) \varphi_{\xi_k}^a(r_1), \quad (9)$$

where ξ_i (ξ_k) is the complete set of quantum numbers n_i, l_i, j_i (n_k, l_k, j_k) identifying the neutron or proton single-particle state involved in the particle (hole) excitation and $\varphi_{\xi_i}^b(r_1)$ [$\varphi_{\xi_k}^a(r_1)$] is the related single-particle wave function. The $C_{L_1SJ_1}^{j_il_ij_kl_k}(ab)$ factors are defined as follows:

$$C_{L_1SJ_1}^{j_il_ij_kl_k}(ab) = \sqrt{6(2j_i+1)}\,\langle l_ij_i||T^{L_1SJ_1}||l_kj_k\rangle \times \sqrt{2J_1+1}\,\mathrm{OBTD}(abj_ij_k, J_1). \quad (10)$$

The tensors $T^{L_1SJ_1}$ are defined by

$$T_{M_J}^{L_1SJ_1} = \sum_{MM_S} i^L Y_{LM} \sigma_{M_S}^S (LMSM_S|JM_J), \quad (11)$$

while the OBTD is defined by

$$\mathrm{OBTD}(abj_ij_k, J_1) = \frac{\langle a \,\|\, [a_{j_i}^\dagger \otimes \tilde{a}_{j_k}]^{J_1} \,\|\, b\rangle}{\sqrt{2J_1+1}}, \quad (12)$$

where $\tilde{a}_{j_k,m_k}$ is related to the annihilation operator a_{j_k,m_k} by $\tilde{a}_{j_k,m_k} = (-)^{j_k+m_k} a_{j_k,-m_k}$, and $\otimes$ is the tensor product.

The radial form factors defined in Eq. (5) were calculated by the computer code FOFA [63] by folding the isovector NN T-matrix with the projectile and target transition densities. In the present analysis, the OBTDs were calculated within the framework of the nuclear shell model using the code KSHELL [64]. Similarly to the case of the sequential transfer, the $p-sd$-mod interaction [53] was adopted for both the $^{18}\mathrm{O} \to {}^{18}\mathrm{F}$ and $^{12}\mathrm{C} \to {}^{12}\mathrm{B}$ transitions. The values of the OBTDs adopted for the $^{18}\mathrm{O} \to {}^{18}\mathrm{F}$ and $^{12}\mathrm{C} \to {}^{12}\mathrm{B}$ unnatural parity transitions are listed in the Supplemental Material (see Ref. [52]) in Tables VI and VII, while the values for the natural parity transitions are listed there in Tables VIII and IX.

The single-particle radial wave functions, entering in the transition densities of Eq. (9), were calculated considering the single particles (or single holes) bound to the core by means of a Woods-Saxon potential. For $^{18}\mathrm{O} + (\pi_{nlj})$ and $^{18}\mathrm{F} + (\nu_{nlj})^{-1}$, the 1.26 fm reduced radius and 0.7 fm diffuseness were adopted, while for $^{12}\mathrm{C} + (\nu_{nlj})$ and $^{12}\mathrm{B} + (\pi_{nlj})^{-1}$, the 1.25 fm reduced radius and 0.65 fm diffuseness were adopted. The depth of the potential was adjusted to reproduce the proton and neutron separation energies of the considered particle or hole. These choices are consistent with those of the two-step transfer reaction mechanism and, in general, are compatible with the typically adopted values [54] for such kind of nuclei.

The effective local nucleon-nucleon interaction potential contains both direct and exchange components, and both central and tensor components parameterized by the sum of three Yukawa functions (M3Y). The M3Y parameters come from a proper interpolation procedure between two different parametrizations, as discussed in Ref. [15] and recently updated in Ref. [43]: (i) the G-matrix calculated by solving the Bethe-Salpeter equation with Paris nucleon-nucleon potential for $E/A \leqslant 10$ MeV [65], and (ii) the Franey-Love parametrization of the effective nucleon-nucleon T-matrix for $E/A \geqslant 100$ MeV [66]. In recently published works (Refs. [35,67]), it was shown how the schematic treatment of the interplay between nuclear structure and hadronic effects

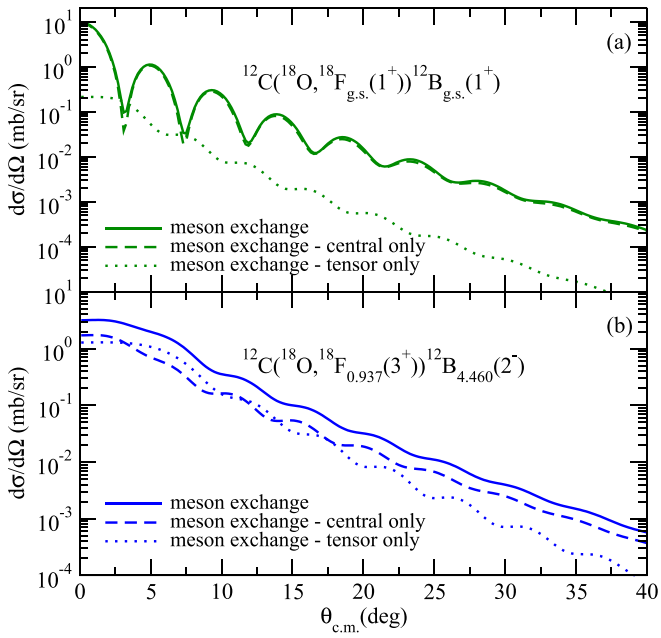

FIG. 5. Angular distribution of differential cross sections for the (a) ^{12}C(^{18}O, ^{18}F$_{g.s.}$(1$^+$)) ^{12}B$_{g.s.}$(1$^+$) and (b) ^{12}C(^{18}O, ^{18}F$_{0.937}$(3$^+$)) ^{12}B$_{4.460}$(2$^-$) SCE reactions. The theoretical curves are evaluated within DWBA calculations of the direct meson-exchange reaction mechanism adopting the CCEP. The calculations with the central (dashed line), tensor (dotted line), and complete (continuous line) nucleon-nucleon interaction are shown separately for each transition.

determines the well-known missing GT strength in the Ikeda sum rule. This quenching can be deduced from the comparison with the experimental data, as done, for example, in Refs. [68,69], or can be obtained from a microscopic theory able to consistently calculate the Hamiltonian and operators as realistic shell-model [70–72] and *ab initio* [73] approaches. Here, we use the empirical average quenching factor extracted from the comparison with the experimental data (≈0.7) to rescale the spin-isospin $S = 1$, $T = 1$ central direct component of the nucleon-nucleon interaction.

Examples of the direct meson-exchange SCE calculations obtained considering the central, tensor, and full nucleon-nucleon interaction are shown in Fig. 5 for the ^{12}C(^{18}O, ^{18}F$_{g.s.}$(1$^+$)) ^{12}B$_{g.s.}$(1$^+$) and the ^{12}C(^{18}O, ^{18}F$_{0.937}$(3$^+$)) ^{12}B$_{4.460}$(2$^-$) transitions. The role of the central and tensor components of the nucleon-nucleon interaction depends on the specific transition, as discussed in detail in Sec. IV.

C. DWBA calculations

The DWBA calculations were performed using the double-folding São Paulo potential (SPP) $V_{SPP}(r)$ [74], both for the real and imaginary parts of the optical potential $U(r) = (N_R + iN_I)V_{SPP}(r)$ assuming the $N_R = 1$ and $N_I = 0.78$ values. The ISI for the ^{18}O + ^{12}C partition and the interactions for the ^{17}O + ^{13}C and ^{19}F + ^{11}B systems were introduced and tested in a previously published work [45]. The same approach was used to describe the final state interaction (FSI) of the ^{18}F + ^{12}B SCE partition. The choice of these parameters was constrained to the robust systematic ones derived from the application of the SPP to the analysis of a wide set of scattering and fusion cross-section data [75]. In this way, no free parameters are available in the choice of optical potentials.

In Ref. [45], it was shown how the introduction of the high-order effects due to the coupling with the first strongly excited inelastic states is crucial to properly describe the elastic scattering cross section in the explored transferred momentum range. This evidence, together with the study of the one-neutron stripping and one-proton pick-up reaction channels, indicated that the ISI needed for the description of all the other quasielastic reaction channels should account for these couplings. In the coupled-channel Born approximation (CCBA) and coupled reaction channel (CRC) calculations presented therein, the sequential transfer SCE reaction mechanism was also included in the calculation, even though only a small number of ^{12}B and ^{18}F levels was considered, compatibly with the available computing power.

The analysis presented in this paper focuses on the SCE reaction channel, and requires (i) the extension of the coupling scheme in terms of ^{12}B and ^{18}F levels, as shown in Fig. 3, and (ii) the treatment of the meson-exchange reaction mechanism consistently included in the cross-section calculation. Although it is among the ambitions of our research project, an extensive inclusion of entrance channel couplings in SCE calculations is a very demanding task, both from the theoretical and computational sides. From the theoretical side, the description of the sequential reaction mechanism in a CCBA or CRC approach requires specific developments for the proper treatment of the nonorthogonality terms, while, for the meson-exchange mechanism, further developments are needed to properly define the form factors. Furthermore, the dimension of the coupling scheme in the case of coupled-channel SCE calculations is beyond the computational limit of typically available servers, even for light and low-density-of-state nuclei, such as those studied in this paper. Developments aimed at parallelizing the calculations on server clusters and minimizing the required computing power are underway.

In this framework, the effect of the channel couplings can be effectively incorporated in the optical potential by means of an effective polarization term, as discussed by the authors of Ref. [13], thus obtaining a coupled-channel equivalent potential (CCEP). This approach was used to describe the ^{18}O + ^{12}C elastic and inelastic scattering data in Ref. [76]. In Fig. 6, the cross-section angular distribution extracted for peak 1 is compared to the C(^{18}O, ^{18}F$_{g.s.}$(1$^+$)) ^{12}B$_{g.s.}$(1$^+$) full reaction mechanism SCE calculations, adopting the SPP and the CCEP.

The cross-section angular distributions have been calculated in DWBA both for the direct and sequential reaction mechanisms and are shown in Fig. 2 for the five regions of interest (ROIs) highlighted in Fig. 1, adopting the coupling scheme shown in Fig. 3. The theoretical curves for each peak (i) were obtained by the weighted sum of each angular distribution ($\frac{d\sigma_j}{d\Omega}$) calculated for all the transitions (j) included in the coupling scheme (CS), using the following

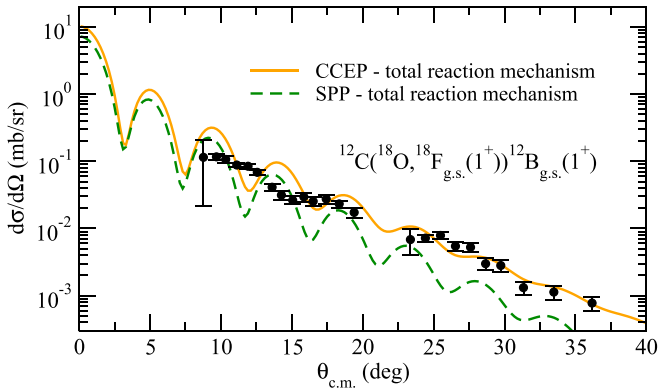

FIG. 6. Experimental cross-section angular distribution of the $^{12}C(^{18}O, ^{18}F_{g.s.})^{12}B_{g.s.}$ single-charge-exchange reaction at 275 MeV beam incident energy. Theoretical calculations for the full reaction mechanism performed adopting the SPP and the CCEP are shown by the green dashed and orange continuous lines, respectively.

formula:

$$\frac{d\sigma_{\text{peak}i}}{d\Omega}(\theta_{\text{c.m.}}) = \sum_{j\in\text{CS}} w_{ij}\frac{d\sigma_j}{d\Omega}(\theta_{\text{c.m.}}). \tag{13}$$

The w_{ij} weights were calculated by the following integral:

$$w_{ij} = \int_{E_{x\_i}^{\min}}^{E_{x\_i}^{\max}} \frac{1}{\sqrt{2\pi}\sigma_j} e^{-\frac{(E_x - E_x^j)^2}{2\sigma_j^2}} dE_x, \tag{14}$$

calculated in the E_x ranges of each peak i assuming for the spectral distribution a normal Gaussian distribution centered at the E_x^j experimental excitation energy for the transition j and the width σ_j assigned as the achieved experimental resolution, also taking into account the Doppler broadening effect, where present. The $\frac{d\sigma_{\text{peak}i}}{d\Omega}(\theta_{\text{c.m.}})$ were finally folded with the experimental angular resolution $\delta\theta_{\text{c.m.}} \approx 0.8^\circ$ to be properly compared to the data.

Another way to compare the measured cross sections with the theoretical calculations is presented in Fig. 7, where the spectral distributions of differential cross section $d\sigma/dE$ are plotted as a function of the E_x excitation energy. The cross-section distribution for the measured experimental data is compared to the direct, sequential, and full reaction mechanism theoretical cross sections. The theoretical spectra are obtained by summing Gaussian spectral distributions for all the possible transitions included within the CS. The parameters of the Gaussian distributions were set in the same way as described in Eq. (14). The theoretical cross sections, integrated in the same angular range of the experimental spectrum, are used to define the heights. Above the S_n threshold, an additional component is added to the spectrum in Fig. 7. It includes the nonresonant one-neutron breakup continuum and the resonant contribution from the spin-dipole resonance (7.6 MeV), giant dipole resonance (7.8 MeV), and the giant quadrupole resonance (12.8 MeV). All of them are combined to the states of the ^{18}F ejectile included in the CS. This part of the spectrum was fitted through a χ^2 minimization procedure on the experimental data, in the energy region $E_x > 6$ MeV,

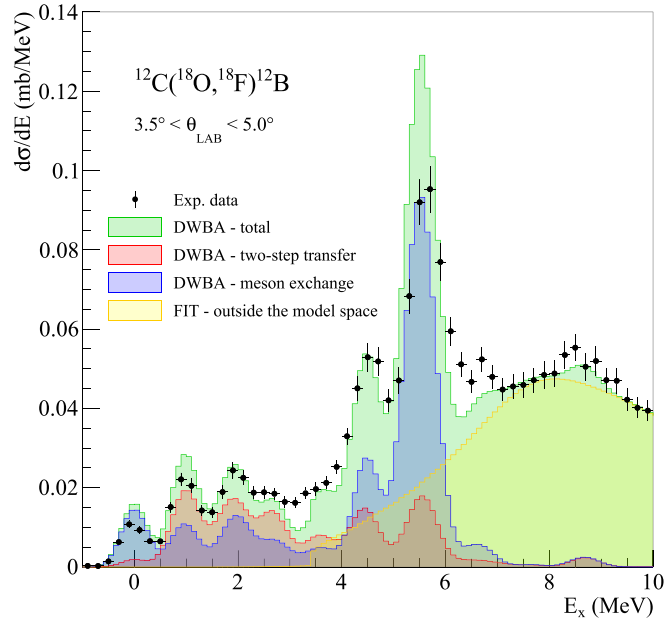

FIG. 7. Spectral distribution of the differential cross section for the $^{12}C(^{18}O, ^{18}F)^{12}B$ SCE reaction at 275 MeV beam incident energy and $3.5^\circ < \theta_{\text{lab}} < 5.0^\circ$. Red and blue hatched areas refer to the meson-exchange and sequential transfer theoretical distributions, respectively; yellow hatched area corresponds to the fit of the resonant and nonresonant contributions above the S_n threshold (see text); green hatched area is the sum of the full reaction mechanism calculation and the fitted yellow spectrum.

and, subsequently, summed to the full reaction mechanism theoretical spectrum.

IV. DISCUSSION

Experimental angular distributions for the five mentioned peaks are shown in Fig. 2 in comparison with the DWBA calculations described in the previous section. The competition among the direct meson exchange and the sequential nucleon transfer reaction mechanisms is visible therein, together with the coherent sum of the two mechanisms. The good agreement between the theoretical and experimental cross sections is notable, considering the high degree of complexity of the complete reaction mechanism and the fact that no arbitrary scaling factor is applied to the calculations. The diffraction pattern of the theoretical curves fairly well reproduces the experimental data, although some differences could be noticed from a detailed comparison. In the case of peak 1 populating the ground state of the $^{18}F + ^{12}B$ system, the calculations predict strong oscillations out of phase with respect to the data. This discrepancy suggests the possible role of alternative reaction paths interfering with the dominant ground-to-ground-state one considered in the present DWBA calculations. Contributions are expected from the meson-exchange reaction mechanism involving the 2^+ and 3^- excited states in the entrance partition, as core-excited intermediate states. The exact treatment of these contributions, although it is among the ambitions of our research project, is nowadays

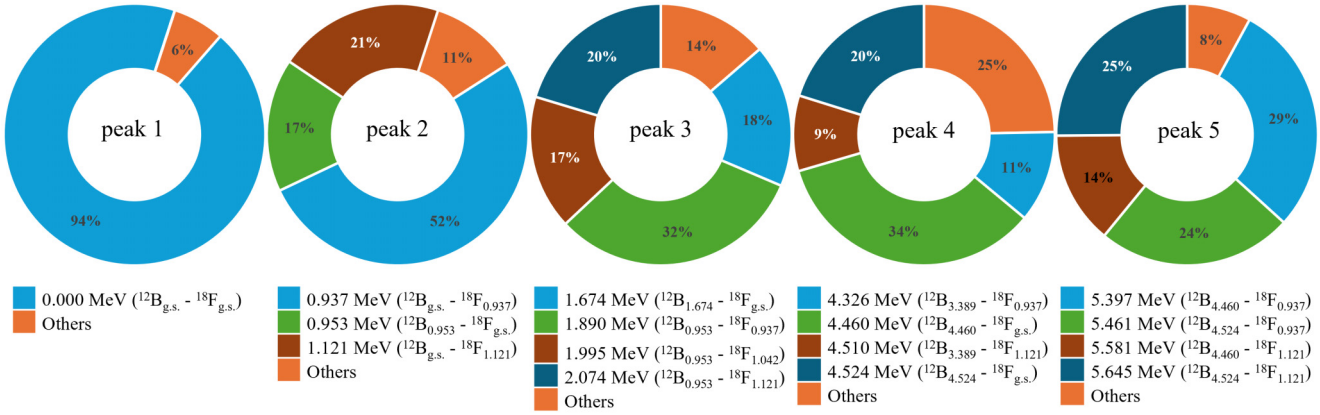

FIG. 8. Composition of the five peaks based on the total coherent sum of all possible SCE reaction mechanisms and calculations described in the present paper. Cross sections are integrated in the angular range $3.5^\circ < \theta_{lab} < 13.4^\circ$ and in the excitation energy ranges shown in Fig. 1.

not feasible and requires some developments that are still ongoing.

Among the large number of transitions included in the adopted CS, it would be interesting to investigate to what extent each of them contributes to the calculated cross section. To this purpose, the composition of the peaks is shown in terms of the populated ejectile and residual nuclear states in Fig. 8. Peak composition comes from the relative theoretical weight of each transition in the five peaks of the theoretical spectrum of Fig. 1, including both the meson-exchange and the sequential transfer components, evaluated in the full angular range $3.5^\circ < \theta_{lab} < 14.3^\circ$. From this analysis, it appears that the bulk of the spectrum for the $^{12}C(^{18}O, ^{18}F)^{12}B$ SCE reaction up to $E_x = 7$ MeV can be described in terms of 15 transitions, involving 4 states of the ejectile and 5 states of the residual nucleus. In particular, the unnatural parity states of the ^{18}F ejectile (1^+ at $E_x = 0.000$ MeV, 3^+ at $E_x = 0.937$ MeV, and 5^+ at $E_x = 1.121$ MeV) and the ^{12}B residual nucleus (1^+ at $E_x = 0.000$ MeV, 2^- at $E_x = 1.674$ MeV, 2^- at $E_x = 4.460$ MeV, and 4^- at $E_x = 4.524$ MeV) dominate the SCE reaction spectrum. This is a general property of the SCE reactions, as commonly observed in other systems [35]. Among such unnatural parity states, further enhancement corresponds to the higher spin states, provided that the angular momentum transferred in the projectile-to-ejectile transition matches the one of the target-to-residual transition. An example of this effect is visible in the composition of peak 5 (see Fig. 8), in which the population of the ^{18}F 3^+ state slightly enhances in ^{12}B the 2^- at 4.460 MeV with respect to the 4^- at 4.524 MeV, while in the case of the population of the ^{18}F 5^+ state, the 4^- state is largely favored. On the same footing, in peak 1, when the $0^+ \rightarrow 1^+$ ground-to-ground-state transition occurs in the ^{12}B nucleus, the population of the 3^+ state of ^{18}F is enhanced at the expense of the 5^+ one. In general, the dominance of the 3^+ states at 0.937 MeV among the states of the ^{18}F ejectile is clearly evident and was also observed at the same incident energy in the $^{40}Ca(^{18}O, ^{18}F)^{40}K$ reaction analyzed in Refs. [14] and [44].

Regarding the natural parity transitions, the only ^{18}F state appearing in the spectrum is the 0^+ isobaric analog state of the ^{18}O ground state at 1.042 MeV. However, its population is suppressed both in the meson exchange, since a natural parity transition is required to also occur in the target-residual side, and in the sequential reaction mechanism, where larger spin transfers are typically favored. For this reason, this 0^+ state of ^{18}F relevantly appears in the SCE spectrum at $E_x = 1.995$ MeV, corresponding to the simultaneous excitation of the ^{12}B 2^+ natural parity state at 0.953 MeV. From the target side, the most relevant natural parity states are the 2^+ and the 3^- at 0.953 and 3.389 MeV, respectively. Being their population is enhanced by the large spin transfer, those states are mostly fed by the sequential nucleon transfer reaction mechanism in composition with the 3^+ and 5^+ ^{18}F unnatural parity states appearing in peaks 3 and 4.

The comparison between the experimental and theoretical integrated cross sections for the sum of all the states belonging to each peak is listed in Table I. Discrepancies lower than 30% between the measured and the theoretical cross sections are obtained for the first three peaks, lying below the one-neutron emission threshold. For these peaks, almost all of the states observed for both the ejectile and the residual nuclei (Ref. [37]) were included in the CS. In the case of peaks 4 and 5, the comparison between the theoretical and the experimental integrated cross sections is slightly worse. This can be explained by the fact that the CS does not include all the possible states at such excitation energies. Moreover,

TABLE I. Experimental and theoretical cross sections integrated in the angular range $3.5^\circ < \theta_{lab} < 13.4^\circ$ and in the excitation energy ranges shown in Fig. 1. Quality factors (QF) evaluated for the total reaction mechanism calculations obtained with the SPP and CCEP.

	$\sigma_{Expt.}$(μb)	$\sigma_{Theo.}$(CCEP)(μb)	QF(SPP)	QF(CCEP)
Peak 1	18 ± 1	24	0.48	0.66
Peak 2	43 ± 1	42	0.47	0.59
Peak 3	47 ± 1	36	0.42	0.51
Peak 4	114 ± 2	68	0.37	0.45
Peak 5	216 ± 3	174	0.45	0.52

contributions above S_n are also expected from the nonresonant one-neutron emission continuum and from the spin-dipole ($E_x = 7.6$ MeV), giant dipole ($E_x = 7.8$ MeV), and giant quadrupole ($E_x = 12.8$ MeV) resonances with widths of 2.1, 4.0, and 3.5 MeV, respectively. These contributions were not included in the calculations since the adopted nuclear structure and reaction theories are not the proper frameworks to describe these collective phenomena. All of these states, properly coupled to the ejectile excitations, were included in the yellow spectrum in Fig. 7 resulting from a fitting procedure that was applied to the experimental data at $E_x > 6$ MeV. From this study, it is clear that the role of these contributions in peaks 4 and 5 is substantial, although the overall good agreement in the comparison between the experimental data and the theoretical calculations suggests a dominance of the 2^- and 4^- states that were explicitly included in the CS.

The most relevant topic treated in the present study refers to the competition among the meson-exchange and the sequential transfer mechanisms in the ^{12}C(^{18}O, ^{18}F)^{12}B SCE reaction at 275 MeV. Comparative analysis of these two reaction mechanisms can be carried on looking at the angular distributions $d\sigma/d\Omega$ or at the spectral distributions $d\sigma/dE$, shown in Figs. 2 and 7. From these analyses, it is clear that peaks 1, 4, and 5 are dominated by the direct meson-exchange reaction mechanism, while the sequential transfer contributes the most in the case of peaks 2 and 3. Therefore, it is concluded that at 15 A MeV incident energy, both reaction mechanisms significantly contribute to the SCE reaction channel. The weight of the two reaction mechanisms for each transition depends on the microscopic nature of the transition itself.

The role of the nucleon-nucleon interaction central and tensor components and their competition is an interesting aspect to investigate, especially in the case of the transitions lying in peaks 1, 4, and 5 in which the meson-exchange reaction mechanism is the most relevant. The central part of the nucleon-nucleon interaction results contributes the most in the $0^+ \rightarrow 1^+$ ground-to-ground-state transition, as visible in Fig. 5(a). In the case of peaks 4 and 5, dominated by the ^{12}C(^{18}O, ^{18}F$_{g.s.}(1^+)$)^{12}B$_{4.460}(2^-)$ and the ^{12}C(^{18}O, ^{18}F$_{0.937}(3^+)$)^{12}B$_{4.460}(2^-)$ transitions, respectively, a major role is instead played by the tensor part [see Fig. 5(b)]. These results can be interpreted by the typically observed phenomenology, in which the role of the tensor interaction is enhanced in the case of spin-flip transitions involving larger transferred total angular momenta.

In the case of the transitions below peaks 2 and 3, in which the sequential nucleon transfer reaction mechanism is the most relevant, it is interesting to study the relative weight of the *pn*-sce and *np*-sce reaction paths. Figure 4 shows that the *np* path, compared to the *pn* one, gives a larger contribution to the sequential transfer SCE cross section, both in the case of the ^{12}C(^{18}O, ^{18}F$_{0.937}(3^+)$)^{12}B$_{g.s.}(1^+)$ and the ^{12}C(^{18}O, ^{18}F$_{0.937}(3^+)$)^{12}B$_{0.953}(2^+)$ transitions dominating peaks 2 and 3, respectively.

A quantitative approach to evaluate the agreement of the obtained theoretical results with the experimental data consists in the quality factor analysis introduced in Ref. [45]. Here this analysis is extended to the case of the SCE reaction data and calculations. The QF (see Eq. (5) in Ref. [45]) was calculated for each measured angular distribution in comparison to the values of the theoretical DWBA calculations adopting the SPP and CCEP, and the obtained values are listed in Table I.

A quantitative approach to evaluate the agreement of the obtained theoretical results with the experimental data consists in the quality factor analysis introduced in Ref. [45]. The quality factor is calculated for each cross-section experimental data point using Eq. (4) in Ref. [45], in comparison to the theoretical DWBA value calculated adopting the SPP and the CCEP optical potentials. The proposed quality factor has the advantage to equally weigh all the points of each angular distribution, regardless of their absolute value. This is a fundamental feature for distributions with an exponential slope, such as the differential cross-section angular distributions. The values of the quality factor range between 0 and 1, corresponding to the worst and best agreements between the calculations and the experimental data, respectively. Small discrepancies around $\sigma_{exp} = \sigma_{theo}$ imply large changes in the QF. As an example, from $\sigma_{exp}/\sigma_{theo} = 1.2$ to $\sigma_{exp}/\sigma_{theo} = 2$, the quality factor moves from 0.85 to 0.59. On the contrary, for large discrepancies ($\sigma_{exp}/\sigma_{theo}$ from 1000 to 10 000), variations in the QF are smaller (0.12 to 0.10). This property allows one to amplify the scale of the quality factor in the case of descriptions that are close to the experimental data and to relax it in the case of calculations that are very distant from the experimental data. The quality factors are averaged on the entire angular distribution (see QF definition from Eq. (5) in Ref. [45]) and then on the entire reaction channel (see ⟨QF⟩ definition from Eq. (6) in Ref. [45]).

Here the quality factor analysis is applied to the case of the SCE reaction channel and the obtained values are listed in Table I. From the values of QF reported therein, it appears evident that the role played by the ISI in SCE reactions is crucial. In fact, for all peaks, the introduction of the CCEP leads to a significant improvement in the quality factor. As one would expect based on the completeness of the adopted CS, the description of the data is better in the case of peaks with smaller excitation energy, where the level density is lower, only bound states could be populated, and core-excitation configurations are expected to give a smaller contribution. The role of CCEP in improving the description of the experimental data up to large scattering angles was already evident in Fig. 6. This feature is typical in the elastic scattering analysis, where the effects due to couplings with the inelastic scattering states and, consequently, the changes in the distortion factor are more evident at larger transferred momenta.

The ⟨QF⟩ was calculated as the average of the several values obtained from all the angular distributions competing to a specific reaction channel. The values of ⟨QF⟩ obtained for the elastic scattering, one-neutron stripping, one proton pick-up, and SCE are shown in Fig. 9, as resulted from the DWBA analysis adopting the SPP and the CCEP. In the case of SCE, peaks 4 and 5 on the unbound region of the spectrum were not included in the ⟨QF⟩ evaluation due to the lack of treatment of the resonant and nonresonant continuous components. From the comparison of the ⟨QF⟩ s obtained

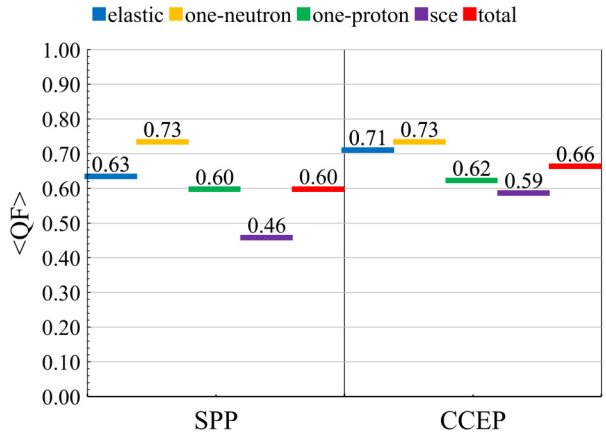

FIG. 9. Average quality factors extracted according to Eq. (5) of Ref. [45] in the experimentally explored angular range for the elastic scattering, one-neutron stripping, one-proton pick-up, and single-charge-exchange reaction channels, and for the DWBA calculations obtained with the two adopted SPP and CCEP. The total value related to the complete network of nuclear reactions is also shown (see text).

for the four reaction channels, we observe how the description of the SCE reaction channel is as good as the others. This is a very important result, taking into account the much higher complexity of the SCE reaction mechanism compared to the other reaction channels. However, this result can be obtained in DWBA when considering the CCEP. Reaction channels other than the elastic scattering and the SCE are only slightly affected by the introduction of the CCEP. This result underlines how the features of the SCE reaction channel are more similar to those of the elastic scattering than to the transfer ones and requires the appropriate treatment of the distortion factor.

In Fig. 9, the ⟨QF⟩ value corresponding to the whole network of nuclear reactions and data analysis is reported and labeled as total.

V. CONCLUSIONS

The ^{12}C(^{18}O, ^{18}F)^{12}B SCE reaction at 275 MeV beam incident energy was studied in a consistent multichannel approach both from the experimental and theoretical sides, with emphasis on the competition between the direct meson-exchange and the sequential nucleon transfer reaction mechanisms. The ^{12}C(^{18}O, ^{18}O)^{12}C elastic and inelastic scattering, the ^{12}C(^{18}O, ^{17}O)^{13}C one-neutron stripping, and the ^{12}C(^{18}O, ^{19}F)^{11}B one-proton pick-up reactions were explored under the same experimental conditions and the results were previously published in Ref. [45].

The absolute cross-section angular and spectral distributions were measured in a wide range at forward scattering angles and up to 10 MeV in excitation energy. The achieved energy ($\delta E_x \approx 0.6$ MeV) and angular ($\delta\theta_{\mathrm{c.m.}} \approx 0.8^\circ$) resolution allowed one to isolate the ground-to-ground-state transition and to map the diffraction patterns in the angular distributions. Three structures have been observed in the spectrum below the neutron emission threshold at 3.370 MeV, while the most prominent peaks are above that threshold, at about 4.5 and 5.5 MeV.

The experimental data were analyzed with state-of-the-art methods of quantum scattering theory in the DWBA approximation, coherently treating both the meson-exchange and the sequential transfer reaction mechanisms. The initial (ISI) and final (FSI) state nucleus-nucleus interactions, as well as the one for the intermediate partitions, adopted in the calculations, were treated in a double-folding approach adopting the SPP both for the real and the imaginary parts. The coupled-channel effects in the initial partition were effectively taken into account, adopting a properly derived coupled-channel equivalent potential from the elastic scattering data analysis. Nuclear structure inputs, for both the meson exchange and the sequential transfer, were extracted from large-scale shell-model calculations adopting the $p - sd - mod$ interaction, while keeping a high degree of consistency in the multichannel analysis.

Despite the large amount of linear momentum available, giving access to a wide range of multipolarities, the ^{12}C(^{18}O, ^{18}F)^{12}B SCE reaction at 275 MeV turned out to be a very selective nuclear process. In general, the direct meson-exchange reaction mechanism favors the unnatural parity transitions, while in the sequential transfer, the higher multipolarities are typically enhanced. Further selectivity comes from parity conservation and from the matching among the transferred orbital angular momentum between the projectile-like and the targetlike nuclei. Indeed, in spite of the large number of available nuclear states of both ejectile and residual nucleus included in the coupling scheme, only 15 transitions are sufficient to obtain an appreciably good description of the spectrum up to $E_x = 7$ MeV.

The quality factor analysis allows one to obtain a quantitative evaluation of the agreement between the experimental data and the adopted theory. A decline of the agreement is observed above the neutron emission threshold, where the adopted theory does not allow one to treat the continuum components of the spectrum. As one would have expected, restrictions on the model space become relevant with the increasing density of states, and their impact is reflected on the comparison between the theoretical model and the experimental data. However, the QF obtained for the entire reaction channel in the bound state region is comparable with what is obtained for the elastic scattering and nucleon transfer reaction channels. This result, in light of the high degree of complexity of the study given by the manifold nature of the SCE reaction mechanism, is encouraging.

Besides the data provided here, the main contribution of this manuscript is the consistent microscopic analysis of the SCE reaction, which includes both the sequential nucleon transfer routes as well as the meson-exchange mechanism in a quantum scattering theoretical approach. We found that at the incident energy of the present experiment (15 A MeV), the three individual components to the SCE cross section are typically relevant, so that it is essential to treat them altogether. Going to finer details, we observe a pronounced state dependence on the relative weight of the three reaction mechanisms, with some transitions more favorably fed by meson exchange

and other by two-step nucleon transfer, making heavy-ion SCE reactions a useful tool for testing nuclear structure models. The agreement of the calculations with the data presented in the manuscript is significantly better than traditional approaches to SCE, where the different reaction mechanisms were either treated separately or one or the other just ignored. Nonetheless, room is left for further improvements, which calls for the extension of the present approach, where coupled-channel effects are treated in average by CCEP, to a full CCBA and/or CRC. This program is still hindered by theoretical issues as well as by limitations in calculation resources, but we are committed to make an attempt along this direction in the near future.

The application of advanced nuclear structure and reaction theories in the multichannel view proposed in this paper results in a promising method for accurate investigations of direct reactions originating in heavy-ion collisions. This is quite appealing for the precise spectroscopy of heavy nuclei proposed in many areas of nuclear physics. An example is the NUMEN project with its challenging commitment to provide valuable information on the $0\nu\beta\beta$ nuclear matrix elements from single- and double-charge-exchange cross-section measurements.

ACKNOWLEDGMENTS

The authors would like to thank all the staff of the LNS Accelerator for the support during the experiments. This project received funding from the European Research Council (ERC) under the European Union's Horizon 2020 research and innovation program (Grant Agreement No. 714625). The NUMEN project is mainly funded by INFN. J.A.L. acknowledges funding by Grant No. MCIN/AEI/10.13039/501100011033 under I + D + i Project No. PID2020-114687GB-I00. L.A., E.R.C.L., and P.A.-V. received funding from the DGAPA-PAPIIT Project No. IG101423. This research was also funded by the Science Committee of the Ministry of Science and Higher Education of the Republic of Kazakhstan (Grant No. AP15473124).

[1] T. Taddeucci, C. Goulding, T. Carey, R. Byrd, C. Goodman, C. Gaarde, J. Larsen, D. Horen, J. Rapaport, and E. Sugarbaker, Nucl. Phys. A **469**, 125 (1987).
[2] F. Osterfeld, Rev. Mod. Phys. **64**, 491 (1992).
[3] V. F. Dmitriev, V. Zelevinsky, and S. M. Austin, Phys. Rev. C **65**, 015803 (2001).
[4] W. P. Alford and B. M. Spicer, Nucleon charge-exchange reactions at intermediate energy, in *Advances in Nuclear Physics*, edited by J. W. Negele and E. Vogt (Springer US, Boston, MA, 2002), pp. 1–82.
[5] D. Frekers, Prog. Part. Nucl. Phys. **57**, 217 (2006).
[6] Y. Fujita, B. Rubio, and W. Gelletly, Prog. Part. Nucl. Phys. **66**, 549 (2011).
[7] G. A. Brischetto, O. Sgouros, D. Carbone, F. Cappuzzello, M. Cavallaro, J. Lubian, G. De Gregorio, C. Agodi, D. Calvo, E. R. Chávez Lomelí, I. Ciraldo, F. Delaunay, H. Djapo, C. Eke, P. Finocchiaro, M. Fisichella, A. Gargano, M. A. Guazzelli, A. Hacisalihoglu, R. Linares *et al.*, Phys. Rev. C **109**, 014604 (2024).
[8] L. La Fauci *et al.* (NUMEN Collaboration), Phys. Rev. C **104**, 054610 (2021).
[9] D. Carbone, R. Linares, P. Amador-Valenzuela, S. Calabrese, F. Cappuzzello, M. Cavallaro, S. Firat, M. Fisichella, A. Spatafora, L. Acosta, C. Agodi, I. Boztosun, G. Brischetto, D. Calvo, E. Chávez Lomelí, I. Ciraldo, M. Cutuli, F. Delaunay, N. Deshmukh, P. Finocchiaro *et al.*, Universe **7**, 58 (2021).
[10] A. Spatafora *et al.* (NUMEN Collaboration), Phys. Rev. C **100**, 034620 (2019).
[11] L. M. Fonseca, R. Linares, V. A. B. Zagatto, F. Cappuzzello, D. Carbone, M. Cavallaro, C. Agodi, J. Lubian, and J. R. B. Oliveira, Phys. Rev. C **100**, 014604 (2019).
[12] V. A. B. Zagatto, F. Cappuzzello, J. Lubian, M. Cavallaro, R. Linares, D. Carbone, C. Agodi, A. Foti, S. Tudisco, J. S. Wang, J. R. B. Oliveira, and M. S. Hussein, Phys. Rev. C **97**, 054608 (2018).
[13] I. Thompson, M. Nagarajan, J. Lilley, and M. Smithson, Nucl. Phys. A **505**, 84 (1989).
[14] M. Cavallaro, J. I. Bellone, S. Calabrese, C. Agodi, S. Burrello, F. Cappuzzello, D. Carbone, M. Colonna, N. Deshmukh, H. Lenske, A. Spatafora, L. Acosta, P. Amador-Valenzuela, T. Borello-Lewin, G. A. Brischetto, D. Calvo, V. Capirossi, E. Chávez, I. Ciraldo, M. Cutuli *et al.*, Front. Astron. Space Sci. **8**, 659815 (2021).
[15] H. Lenske, Nucl. Phys. A **482**, 343 (1988).
[16] M. Toyama, Nucl. Phys. A **277**, 401 (1977).
[17] W. R. Wharton and P. T. Debevec, Phys. Rev. C **11**, 1963 (1975).
[18] J. S. Winfield, N. Anantaraman, S. M. Austin, L. H. Harwood, J. van der Plicht, H.-L. Wu, and A. F. Zeller, Phys. Rev. C **33**, 1333 (1986).
[19] H. Lenske, H. H. Wolter, and H. G. Bohlen, Phys. Rev. Lett. **62**, 1457 (1989).
[20] S. Nakayama, T. Yamagata, K. Yuasa, M. Tanaka, H. Bohlen, H. Lenske, H. Wolter, M. Inoue, T. Itahashi, and H. Ogata, Nucl. Phys. A **507**, 515 (1990).
[21] F. Cappuzzello, H. Lenske, A. Cunsolo, D. Beaumel, S. Fortier, A. Foti, A. Lazzaro, C. Nociforo, S. E. A. Orrigo, and J. S. Winfield, Nucl. Phys. A **739**, 30 (2004).
[22] C. Bertulani, Nucl. Phys. A **554**, 493 (1993).
[23] H. Bohlen, B. Gebauer, D. Kolbert, S. Kubono, W. von Oertzen, P. Pellegrin, E. Stiliaris, M. Wllpert, T. Wilpert, H. Lenske, H. Wolter, A. Miczaika, N. Alamanos, J. Barrette, B. Berthier, B. Fernandez, J. Gastebois, C. Berat, M. Buenerd, J. Hostachy *et al.*, Nucl. Phys. A **488**, 89 (1988).
[24] W. von Oertzen, Nucl. Phys. A **482**, 357 (1988).
[25] S. Nakayama, T. Yamagata, K. Yuasa, M. Tanaka, M. Inoue, T. Itahashi, and H. Ogata, Phys. Lett. B **246**, 342 (1990).
[26] S. Nakayama, H. Akimune, I. Daito, H. Fujimara, Y. Fujita, M. Fujiwara, K. Fushimi, T. Inomata, K. Ishibashi, H. Kohri, N. Koori, K. Takahisha, A. Tamii, M. Tanaka, H. Toyokawa, and T. Yamagata, Phys. Rev. C **60**, 047303 (1999).
[27] T. Annakkage, J. Jänecke, J. Winfield, G. Berg, J. Brown, G. Crawley, S. Danczyk, M. Fujiwara, D. Mercer, K. Pham, D. Roberts, J. Stasko, and G. Yoo, Nucl. Phys. A **648**, 3 (1999).

[28] J. Cook, K. W. Kemper, P. V. Drumm, L. K. Fifield, M. A. C. Hotchkis, T. R. Ophel, and C. L. Woods, Phys. Rev. C **30**, 1538 (1984).

[29] N. Clarke and J. Cook, Nucl. Phys. A **458**, 137 (1986).

[30] F. Cappuzzello, A. Cunsolo, S. Fortier, A. Foti, M. Khaled, H. Laurent, H. Lenske, J. Maison, A. Melita, C. Nociforo, L. Rosier, C. Stephan, L. Tassan-Got, J. Winfield, and H. Wolter, Phys. Lett. B **516**, 21 (2001).

[31] A. Etchegoyen, M. C. Etchegoyen, E. D. Izquierdo, D. Abriola, D. E. Di Gregorio, J. O. Fernández Niello, A. M. J. Ferrero, S. Gil, A. O. Macchiavelli, A. J. Pacheco, and J. E. Testoni, Phys. Rev. C **38**, 2124 (1988).

[32] H. Ejiri, N. Soukouti, and J. Suhonen, Phys. Lett. B **729**, 27 (2014).

[33] L. Jokiniemi, J. Suhonen, and H. Ejiri, Magnetic hexadecapole γ Transitions and neutrino-nuclear responses in medium-heavy nuclei, Adv. High Energy Phys. **2016**, 8417598 (2016).

[34] J. Suhonen and O. Civitarese, Phys. Rep. **300**, 123 (1998).

[35] H. Lenske, F. Cappuzzello, M. Cavallaro, and M. Colonna, Prog. Part. Nucl. Phys. **109**, 103716 (2019).

[36] J. I. Bellone, S. Burrello, M. Colonna, J.-A. Lay, and H. Lenske, Phys. Lett. B **807**, 135528 (2020).

[37] M. Chadwick, P. Obložinský, M. Herman *et al.*, Nucl. Data Sheets **107**, 2931 (2006).

[38] B. T. Kim, A. Greiner, M. A. G. Fernandes, N. Lisbona, K. S. Low, and M. C. Mermaz, Phys. Rev. C **20**, 1396 (1979).

[39] D. Horen, B. Burks, M. Fernandes, R. Auble, F. Bertrand, J. Blankenship, J. L. C. Ford, Jr., E. Gross, D. Hensley, R. Sayer, G. Satchler, D. Shapira, T. Sjoreen, and F. Petrovich, Phys. Lett. B **181**, 38 (1986).

[40] L. Fifield, W. Catford, N. Orr, T. Ophel, A. Etchegoyen, and M. Etchegoyen, Nucl. Phys. A **552**, 125 (1993).

[41] F. Cappuzzello *et al.*, Eur. Phys. J. A **54**, 72 (2018).

[42] F. Cappuzzello, C. Agodi, L. Calabretta, D. Calvo, D. Carbone, M. Cavallaro, M. Colonna, P. Finocchiaro, F. Iazzi, R. Linares, J. R. B. Oliveira, L. Pandola, E. Santopinto, D. Torresi, S. Tudisco, L. Acosta, C. Altana, P. Amador-Valenzuela, L. H. Avanzi, J. Bellone *et al.*, Intl. J. Mod. Phys. A **36**, 2130018 (2021).

[43] F. Cappuzzello, H. Lenske, M. Cavallaro, C. Agodi, N. Auerbach, J. Bellone, R. Bijker, S. Burrello, S. Calabrese, D. Carbone, M. Colonna, G. De Gregorio, J. Ferreira, D. Gambacurta, H. García-Tecocoatzi, A. Gargano, J. Lay, R. Linares, J. Lubian, E. Santopinto *et al.*, Prog. Part. Nucl. Phys. **128**, 103999 (2023).

[44] B. Urazbekov *et al.* (NUMEN Collaboration), Phys. Rev. C **108**, 064609 (2023).

[45] A. Spatafora, D. Carbone, F. Cappuzzello, M. Cavallaro, L. Acosta, C. Agodi, P. Amador-Valenzuela, T. Borello-Lewin, G. A. Brischetto, S. Calabrese, D. Calvo, V. Capirossi, E. R. Chávez Lomelí, I. Ciraldo, G. De Gregorio, F. Delaunay, H. Djapo, C. Eke, P. Finocchiaro, S. Firat *et al.*, companion paper, Phys. Rev. C **107**, 024605 (2023).

[46] F. Cappuzzello *et al.*, Eur. Phys. J. A **52**, 169 (2016).

[47] D. Torresi, O. Sgouros, V. Soukeras, M. Cavallaro, F. Cappuzzello, D. Carbone, C. Agodi, G. Brischetto, S. Calabrese, I. Ciraldo, N. Deshmukh, A. Hacisalihoglu, L. L. Fauci, and A. Spatafora, Nucl. Instrum. Methods Phys. Res., Sect. A **989**, 164918 (2021).

[48] S. Burrello, S. Calabrese, F. Cappuzzello, D. Carbone, M. Cavallaro, M. Colonna, J. A. Lay, H. Lenske, C. Agodi, J. L. Ferreira, S. Firat, A. Hacisalihoglu, L. La Fauci, A. Spatafora, L. Acosta, J. I. Bellone, T. Borello-Lewin, I. Boztosun, G. A. Brischetto, D. Calvo *et al.*, Phys. Rev. C **105**, 024616 (2022).

[49] S. Nakayama, T. Yamagata, M. Tanaka, M. Inoue, K. Yuasa, T. Itahashi, H. Ogata, N. Koori, and K. Shima, Phys. Rev. Lett. **67**, 1082 (1991).

[50] I. J. Thompson, Comput. Phys. Rep. **7**, 167 (1988).

[51] G. Satchler, *Direct Nuclear Reactions*, International Series of Monographs on Physics, Vol. 68 (Clarendon Press, Oxford, UK, 1983).

[52] See Supplemental Material at http://link.aps.org/supplemental/10.1103/PhysRevC.110.064612 for spectroscopic amplitudes and one-body transition densities.

[53] Y. Utsuno and S. Chiba, Phys. Rev. C **83**, 021301(R) (2011).

[54] N. Anyas-Weiss, J. Cornell, P. Fisher, P. Hudson, A. Menchaca-Rocha, D. Millener, A. Panagiotou, D. Scott, D. Strottman, D. Brink, B. Buck, P. Ellis, and T. Engeland, Phys. Rep. **12**, 201 (1974).

[55] S. Calabrese *et al.* (NUMEN Collaboration), Phys. Rev. C **104**, 064609 (2021).

[56] O. Sgouros *et al.* (NUMEN Collaboration), Phys. Rev. C **104**, 034617 (2021).

[57] O. Sgouros, M. Cutuli, F. Cappuzzello, M. Cavallaro, D. Carbone, C. Agodi, G. De Gregorio, A. Gargano, R. Linares, G. A. Brischetto, D. Calvo, E. R. Chávez Lomelí, I. Ciraldo, F. Delaunay, H. Djapo, C. Eke, P. Finocchiaro, M. Fisichella, M. A. Guazzelli, A. Hacisalihoglu *et al.*, Phys. Rev. C **108**, 044611 (2023).

[58] I. Ciraldo, F. Cappuzzello, M. Cavallaro, D. Carbone, S. Burrello, A. Spatafora, A. Gargano, G. De Gregorio, R. I. Magana Vsevolodovna, L. Acosta, C. Agodi, P. Amador-Valenzuela, T. Borello-Lewin, G. A. Brischetto, S. Calabrese, D. Calvo, V. Capirossi, E. R. C. Lomelí, M. Colonna, F. Delaunay *et al.*, Phys. Rev. C **105**, 044607 (2022).

[59] I. Ciraldo, F. Cappuzzello, M. Cavallaro, D. Carbone, A. Gargano, G. De Gregorio, H. Garcia-Tecocoatzi, E. Santopinto, R. I. Magaña-Vsevolodovna, L. Acosta, C. Agodi, P. Amador-Valenzuela, G. A. Brischetto, S. Burrello, D. Calvo, E. R. Chávez Lomeli, M. Colonna, F. Delaunay, H. Djapo, C. Eke *et al.*, Phys. Rev. C **109**, 024615 (2024).

[60] I. J. Thompson, Reaction mechanisms of pair transfer, in *Fifty Years of Nuclear BCS* (World Scientific, 2013), pp. 455–467.

[61] H. Lenske, J. I. Bellone, M. Colonna, and J. A. Lay, Phys. Rev. C **98**, 044620 (2018).

[62] A. Etchegoyen, D. Sinclair, S. Liu, M. Etchegoyen, D. Scott, and D. Hendrie, Nucl. Phys. A **397**, 343 (1983).

[63] H. Lenske (private communication).

[64] N. Shimizu, T. Mizusaki, Y. Utsuno and Y. Tsunoda, Comput. Phys. Commun. **244**, 372 (2019).

[65] N. Anantaraman, H. Toki, and G. Bertsch, Nucl. Phys. A **398**, 269 (1983).

[66] M. A. Franey and W. G. Love, Phys. Rev. C **31**, 488 (1985).

[67] D. Gambacurta and M. Grasso, Phys. Rev. C **105**, 014321 (2022).

[68] M. J. G. Borge, P. G. Hansen, B. Jonson, S. Mattsson, G. Nyman, A. Richter, and K. Riisager, Z. Phys. A **332**, 413 (1989).

[69] G. Martínez-Pinedo, A. Poves, E. Caurier, and A. P. Zuker, Phys. Rev. C **53**, R2602 (1996).

[70] L. Coraggio, N. Itaco, G. De Gregorio, A. Gargano, Z. H. Cheng, Y. Z. Ma, F. R. Xu, and M. Viviani, Phys. Rev. C **109**, 014301 (2024).
[71] L. Coraggio, N. Itaco, G. De Gregorio, A. Gargano, R. Mancino, and F. Nowacki, Phys. Rev. C **105**, 034312 (2022).
[72] L. Coraggio, L. De Angelis, T. Fukui, A. Gargano, N. Itaco, and F. Nowacki, Phys. Rev. C **100**, 014316 (2019).
[73] P. Gysbers, G. Hagen, J. D. Holt, G. R. Jansen, T. D. Morris, P. Navrátil, T. Papenbrock, S. Quaglioni, A. Schwenk, S. R. Stroberg, and K. A. Wendt, Nat. Phys. **15**, 428 (2019).
[74] L. C. Chamon, B. V. Carlson, L. R. Gasques, D. Pereira, C. De Conti, M. A. G. Alvarez, M. S. Hussein, M. A. Candido Ribeiro, E. S. Rossi, Jr., and C. P. Silva, Phys. Rev. C **66**, 014610 (2002).
[75] M. Alvarez, L. Chamon, M. Hussein, D. Pereira, L. Gasques, E. Rossi, Jr., and C. Silva, Nucl. Phys. A **723**, 93 (2003).
[76] A. Spatafora (unpublished).